Available online at www.sciencedirect.com
ScienceDirect
Biochimica et Biophysica Acta 1778 (2008) 423–432
Biochimica et Biophysica Acta
BBA
www.elsevier.com/locate/bbamem

MITO-Porter: A liposome-based carrier system for delivery of macromolecules into mitochondria via membrane fusion

Yuma Yamada [a], Hidetaka Akita [a], Hiroyuki Kamiya [a], Kentaro Kogure [a], Takenori Yamamoto [b], Yasuo Shinohara [b], Kikuji Yamashita [c], Hideo Kobayashi [d], Hiroshi Kikuchi [d], Hideyoshi Harashima [a,*]

[a] *Laboratory for Molecular Design of Pharmaceutics, Faculty of Pharmaceutical Sciences, Hokkaido University, Kita-12, Nishi-6, Kita-ku, Sapporo 060-0812, Japan*
[b] *Institute for Genome Research, The University of Tokushima, 3-18 Kuramoto-cho, Tokushima, 770-8503, Japan*
[c] *Institute of Health Biosciences, The University of Tokushima, 3-18 Kuramoto-cho, Tokushima, 770-8504, Japan*
[d] *Daiichi Pharmaceutical Co., Ltd., Tokyo R&D Center 16-13, Kita-Kasai 1-Chome, Edogawa-ku, Tokyo 134-8630, Japan*

Received 12 April 2007; received in revised form 11 October 2007; accepted 2 November 2007
Available online 12 November 2007

Abstract

Mitochondria are the principal producers of energy in higher cells. Mitochondrial dysfunction is implicated in a variety of human diseases, including cancer and neurodegenerative disorders. Effective medical therapies for such diseases will ultimately require targeted delivery of therapeutic proteins or nucleic acids to the mitochondria, which will be achieved through innovations in the nanotechnology of intracellular trafficking. Here we describe a liposome-based carrier that delivers its macromolecular cargo to the mitochondrial interior via membrane fusion. These liposome particles, which we call MITO-Porters, carry octaarginine surface modifications to stimulate their entry into cells as intact vesicles (via macropinocytosis). We identified lipid compositions for the MITO-Porter which promote both its fusion with the mitochondrial membrane and the release of its cargo to the intra-mitochondrial compartment in living cells. Thus, the MITO-Porter holds promise as an efficacious system for the delivery of both large and small therapeutic molecules into mitochondria.

Keywords: Non-viral vector; Mitochondria; Mitochondrial drug delivery; MITO-Porter; Membrane fusion; Octaarginine

1. Introduction

Mitochondrial dysfunction has recently been implicated in a variety of diseases, including cancer, Alzheimer's disease, Parkinson's disease, and diabetes mellitus [1,2]. Although therapies for these diseases are desired, strategies designed to complement mitochondrial dysfunction are rare [3–6]. Targeted delivery of an engineered gene or gene product to the nucleus or mitochondrion is an essential first step towards therapeutic restoration of a missing cellular function [3,7]. For example, a nuclear localization signal (NLS) peptide can be used to guide a protein into the nucleus [8]. However, the same NLS does not work as such when attached to a large circular DNA (i.e., plasmid DNA; pDNA) [9,10]. We also faced this problem in the case of delivery of molecules to mitochondria: conjugation of a mitochondrial targeting signal (MTS) peptide to exogenous proteins and small linear DNAs was found to aid their delivery to the mitochondria [11–15], but this strategy did not work for pDNA. Because large molecules such as pDNA and folded protein do not readily pass through the mitochondrial membrane, they cannot be delivered into mitochondria easily [16,17].

Here, we describe MITO-Porter, a liposome-based carrier that introduces cargos into mitochondria via a membrane fusion mechanism (Fig. 1). The first barrier to intracellular targeting is the plasma membrane. The MITO-Porter surface carries octaarginine (R8) moieties at high density so that the particles are internalized by macropinocytosis rather than by clathrin-mediated endocytosis as occurs in the case of cationic liposomes [18]. We have shown that high-density R8-modified liposomes (R8-LPs)

* Corresponding author. Tel.: +81 11 706 3919; fax: +81 11 706 4879.
E-mail address: harasima@pharm.hokudai.ac.jp (H. Harashima).

0005-2736/$ - see front matter © 2007 Elsevier B.V. All rights reserved.
doi:10.1016/j.bbamem.2007.11.002

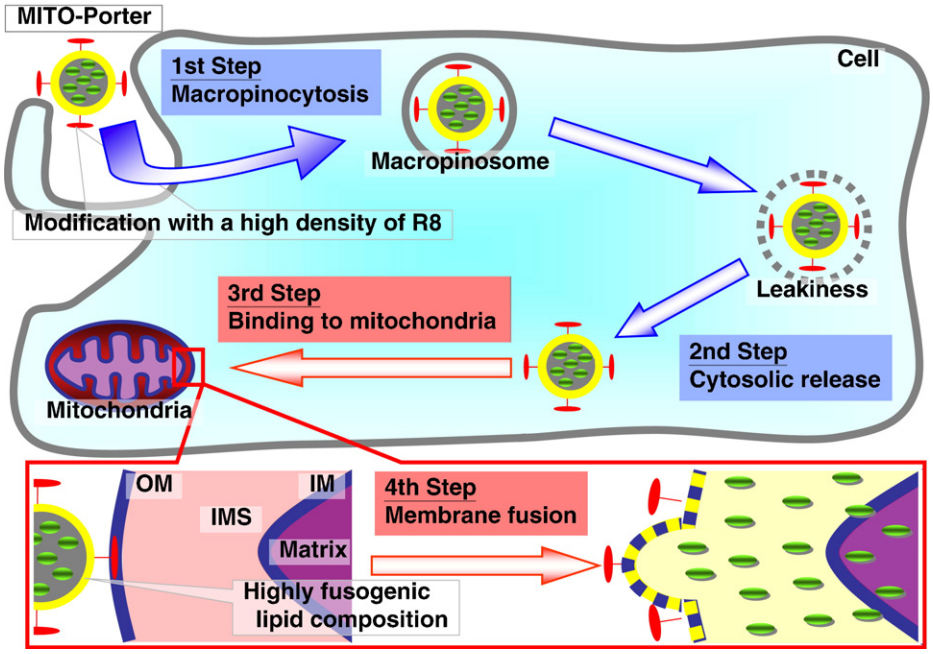

Fig. 1. A new concept for delivery of macromolecules into mitochondria using MITO-Porter. MITO-Porter is surface-modified with a high density of octaarginine (R8), which can be internalized by cells via macropinocytosis (1st step). R8 can escape from macropinosomes to the cytosol, which prevents lysosomal degradation (2nd step). MITO-Porter in the cytosol can bind to mitochondria via electrostatic interactions with R8 (3rd step). Encapsulated compounds are delivered to the intramitochondrial compartment via membrane fusion with the help of sphingomyelin (SM) or phosphatidic acid (PA), which were determined to be fusogenic lipids with the mitochondrial membrane (4th step). OM, outer membrane; IMS, intermembrane space; IM, inner membrane.

can escape from macropinosomes efficiently to the cytosol keeping the encapsulated compounds intact, while low density R8-LPs are taken up via clathrin-mediated endocytosis and degraded by lysosomal enzymes [18]. Upon release from the macropinosomes, MITO-Porter then binds to the mitochondrial membrane via electrostatic interactions, which induces fusion between the MITO-Porter and mitochondrion (Fig. 1).

The purpose of this study was to validate the principle of our mitochondrial delivery system based on membrane fusion. We first screened for liposomes that efficiently fuse with isolated rat liver mitochondria. This was achieved by varying the lipid composition of a panel of liposomes and monitoring membrane fusion by fluorescence resonance energy transfer (FRET) analysis. Two highly fusogenic lipid compositions were identified and they form the basis of the MITO-Porter. Green fluorescence protein (GFP) was used as a model macromolecule, which permitted us to check its delivery to mitochondria by confocal laser scanning microscopic analysis. In addition, membrane fusion between the MITO-Porter and mitochondria in living cells was evaluated by FRET analysis using a spectral imaging fluorescent microscopy system.

2. Materials and methods

2.1. Materials

E. coli strain BL21 (DE3) [F^-, *ompT, hsdS*$_B$ ($r_B^- m_B^-$), *gal, dcm* (DE3)] was purchased from Stratagene (La Jolla, CA, USA). Oligonucleotides were purchased from Sigma Genosys Japan (Ishikari, Japan) in purified form. Adult male Wistar rats (6–10 weeks old) were purchased from Sankyo Labo Service (Sapporo, Japan). Cholesterol (Chol), 1,2-dioleoyl-*sn*-glycero-3-phosphatidyl ethanolamine (DOPE), 7-nitrobenz-2-oxa-1,3-diazole labeled DOPE (NBD–DOPE), and rhodamine–DOPE were purchased from Avanti Polar lipids (Alabaster, AL, USA). Egg yolk phosphatidyl choline (EPC) was obtained from Nippon Oil and Fats Co. (Tokyo, Japan). Cholesteryl hemisuccinate (5-cholesten-3-ol 3-hemisuccinate; CHEMS), cardiolipin (CL), phosphatidic acid (PA), phosphatidyl glycerol (PG), phosphatidyl inositol (PI), phosphatidyl serine (PS), sphingomyelin (SM), and Gold Colloid (8–12nm in diameter; code G-1527) were purchased from Sigma (St. Louis, MO, USA). Stearyl octaarginine (STR-R8) was kindly supplied by Dr. S. Futaki (Kyoto University, Japan). HeLa human cervix carcinoma cells were obtained from RIKEN Cell Bank (Tsukuba, Japan). Dulbecco's modified Eagle medium (D'MEM) and fetal bovine serum (FBS) were purchased from Invitrogen Corp. (Carlsbad, CA, USA). All other chemicals used were commercially available reagent-grade products.

2.2. Preparation of green fluorescent protein

GFP for use as a model macromolecule was prepared as previously described [19]. The purified protein was analyzed by SDS-PAGE. Protein concentrations were determined with a BCA Protein Assay Kit (Pierce; Rockford, IL, USA).

2.3. Liposome preparation

Liposomes were prepared with various lipid compositions by a hydration method (Table 1). Lipid stocks were prepared in chloroform and stored at −20 °C until used. Lipid films were formed on the bottom of a glass tube by evaporating the chloroform solution. To generate empty vesicles, 0.25 mL of mitochondrial isolation buffer [MIB: 250 mM sucrose, 2 mM Tris–HCl, pH 7.4] was applied to 137.5 nmol of dried lipid film. After incubation for 10 min for hydration, the suspensions were sonicated using a bath-type sonicator (85 W, Aiwa Co., Tokyo, Japan) for 15 s. An STR-R8 solution (10 mol% of lipids) was then added to the suspension, followed by incubation for 30 min at room temperature to attach the R8 to the surface of the liposome. The diameter was measured by a quasi-elastic light scattering method, and the zeta potential was determined electrophoretically using an electrophoretic light scattering spectrophotometer (ELS-8000, Otsuka

Table 1
Characteristics of liposomes

Liposome type	Liposome composition (molar ratio)	Lipid X component and diameter of liposomes (nm)							
		Anionic lipids						Neutral lipids	
		CL[b]	PI	PG	PS	PA	CHMES	SM	Chol
R8-DOPE-LP	DOPE[a]:lipid X:STR-R8 (9:2:1)	234±43	224±32	224±25	266±64	261±59	335±27	264±90	260±28
DOPE-LP	DOPE:lipid X (9:2)	318±79	268±33	246±6	289±42	232±56	315±28	223±41	309±29
R8-EPC-LP	EPC:lipid X:STR-R8 (9:2:1)	229±52	218±58	225±38	268±70	217±41	261±34	227±27	279±41
EPC-LP	EPC:lipid X (9:2)	259±69	263±87	307±128	331±72	212±56	336±760	268±32	392±133

[a]DOPE, 1,2-dioleoyl-*sn*-glycero-3-phosphatidyl ethanolamine; EPC, egg yolk phosphatidyl choline; STR-R8, stearyl octaarginine.
[b]CL, cardiolipin; PI, phosphatidyl inositol; PG, phosphatidyl glycerol; PS, phosphatidyl serine; PA, phosphatidic acid; CHEMS, Cholesteryl hemisuccinate (5-cholesten-3-ol 3-hemisuccinate); SM, sphingomyelin; Chol, cholesterol.
Each value is represented by the mean±S.D., $n=3$.

Electronics Co., Ltd; Osaka, Japan). GFP (protein concentration; 125 ng/μL) and Gold Colloid (gold concentration; 0.8 A_{520}) were encapsulated in an aqueous phase as model macromolecules.

To estimate the encapsulation efficiency, GFP encapsulated in liposome containing rhodamine–DOPE was separated from free GFP by centrifugation at 113,000 *g* for 45 min at 4 °C and washed twice in a MIB [20]. The liposome-encapsulated GFP was determined by measuring the fluorescence intensity (excitation at 488 nm and emission at 507 nm) after treatment with lysis buffer (Promega; WI, USA). The amount of the lipid was determined by measuring the fluorescence intensity of rhodamine–DOPE (excitation at 550 nm and emission at 590 nm). The encapsulation efficiency was calculated as follows:

$$\text{encapsulation efficiency } (\%) = (\text{recovered GFP}/\text{ recovered lipid}) / (\text{applied GFP}/\text{applied lipid}) \times 100 \quad (1)$$

2.4. Isolation of mitochondria from rat liver

Mitochondria were isolated from livers obtained from adult male Wistar rats (6–8 weeks old) essentially as described previously [21]. Rats were sacrificed and the livers were removed after bleeding largely subsided, and then placed in approximately 20 mL of ice-cold MIB per 10 g of liver. All subsequent steps were carried out on ice. Livers were chopped into small pieces and the suspension was homogenized in a glass homogenizer (50 mL capacity) with a pestle. Three complete cycles up and down with the pestle were made. The pestle was motor-driven and operated at approximately 550 rpm. The homogenate was diluted approximately 1:3 with MIB and centrifuged at 800 ×*g* for 5 min. The supernatant was transferred into ice-cold tubes and centrifuged at 7500 ×*g* for 10 min. The pellets were washed twice with MIB, which contained EDTA, and once further with EDTA-free MIB. Concentrations of mitochondrial proteins were determined using a BCA protein assay kit. Purity of the mitochondrial preparation was greater than 90% as judged by electron microscopy [22], and the respiration control index of mitochondria was determined to be 4.5–6 using a Clark oxygen-electrode (YSI 5331;Yellow Springs Instrument Co., Yellow Springs, OH, USA), indicating that the mitochondria were intact and respiring. All animal protocols were approved by the institutional animal care and research advisory committee at the Faculty of Pharmaceutical Sciences, Hokkaido University, Sapporo, Japan.

2.5. Membrane fusion assay using FRET analysis

The membrane fusion activity of liposomes with mitochondria was assessed by FRET as described previously [23–25]. In this experiment, liposomes labeled with both 1 mol% NBD–DOPE and 0.5 mol% rhodamine–DOPE were used. A 10-μL aliquot of labeled liposome (lipid concentration, 550 μM) was added to mitochondria isolated from rat liver (0.9 mg of mitochondrial protein/mL) in 90 μL of MIB, and incubated for 30 min at 25 °C. After incubation, energy transfer was assessed by measuring the fluorescence intensity (excitation at 470 nm and emission at 530 nm).

Membrane fusion between the labeled liposomes and the mitochondria will lead to the diffusion of NBD and rhodamine into the lipid membranes, which causes reduction of energy transfer, resulting in an increase in fluorescence intensity at 530 nm. The maximum fluorescence was defined as the fluorescence of liposomes when dissolved in Triton X-100 (final concentration of 0.5%). Fusion activity (%) was estimated by the reduction in the level of energy transfer in accordance with membrane fusion, and was calculated as follows:

$$\text{fusion activity } (\%) = (F - F_0)/(F_{\max} - F_0) \times 100 \quad (2)$$

where F, F_0, $F_{\max}$ represent the fluorescence intensity of labeled liposome after incubation with mitochondria, the fluorescence intensity of labeled liposome after incubation without mitochondria, and the maximum fluorescence intensity after the Triton X-100 treatment, respectively.

2.6. Delivery of GFP to isolated rat liver mitochondria and detection of GFP in mitochondria

A 100-μL aliquot of GFP (125 ng/μL) or GFP encapsulated in R8-LP was individually added to 1 mL of isolated rat liver mitochondria solution (10 mg of mitochondrial protein/mL) to a final lipid concentration of 50 μM and incubated for 30 min at 25 °C. The suspension was centrifuged at 16,000 ×*g* for 10 min at 4 °C to precipitate the mitochondria, and the supernatant was removed. The pellet was washed twice with MIB at 4 °C, and then resuspended in 100 μL of isolation buffer [IB: 70 mM sucrose, 220 mM D-mannitol, 0.5 mg/ml bovine serum albumin (essential fatty acid free, Sigma), 2.0 mM HEPES, pH 7.4].

After incubation, mitochondria were subfractionated into outer membrane (OM) and intermembrane space (IMS) fractions by digitonin treatment followed by differential centrifugation [26]. In brief, an equal volume of IB with 1.25% digitonin (NACALAI TESQUE, INC; Kyoto, Japan) was added to the mitochondria solution and mixed gently for 15 min at 4 °C. The suspension was diluted by the addition of three volumes of IB and then centrifuged at 10,000 ×*g* for 10 min at 4 °C. The pelleted fraction was resuspended in IB and then centrifuged again at 10,000 ×*g* for 10 min at 4 °C. The combined supernatant fluid was centrifuged at 144,000 ×*g* for 60 min at 4 °C. The pelleted fraction was resuspended in 100 μL of IB to obtain the OM fraction. The supernatant was centrifuged again at 144,000 ×*g* for 60 min at 4 °C and the resulting supernatant was used as the IMS fraction. Protein concentrations of both the OM and IMS fractions were determined using a BCA protein assay kit. The protein concentrations were adjusted to 1 mg/mL and stored at −80 °C prior to use. GFP was detected by Western blotting.

2.7. Assessment of degradation of GFP in the mitochondrial intermembrane space

A 10 μL aliquot of GFP (10 ng/μL) was added to 90 μL of either the IMS fraction (1 mg/mL protein concentration) or IB, and then incubated for 30 min at 25 °C. After incubation, the resulting suspensions were stored at −80 °C prior to use. GFP was subject to Western blotting.

A 5-μL aliquot of GFP (125 ng/μL) was added to 50 μL of either the IMS fraction (1 mg/mL) or IB, and incubated for 30 min at 25 °C. After the incubation, an equal volume of IB was added to the resulting suspension and the fluorescence intensity of GFP measured (excitation at 474 nm and emission at 509 nm).

2.8. Western blotting

An equal volume of the sample was mixed with loading buffer (100 mM Tris–HCl (pH 6.8), 4% SDS, 12% 2-mercaptoethanol, 20% glycerol, 0.05% bromophenol blue), and then subjected to 15% SDS-PAGE. After electrophoresis, the proteins were electroblotted onto a Polyvinylidene Fluoride membrane (NIPPON Genetics Co., Ltd; Tokyo, Japan). Antibodies against the N-terminus of GFP derived from rabbit (Sigma) were used at 1:1000 to 1:2500 dilutions. GFP was further detected using secondary HRP-conjugated anti-rabbit antibodies (GE Healthcare UK Ltd, England) at a 1:1000 dilution.

2.9. MITO-Porter transduction and staining of mitochondria for confocal laser scanning microscopy analyses

HeLa cells (4×10^4 cells/mL) were cultured in 35 mm glass base dishes (IWAKI, Tokyo, Japan) with D'MEM, which contained 10% FBS, under 5% CO_2/air at 37 °C for 24 h. The cells were washed with ice-cold phosphate-buffered saline [PBS (−)] and incubated in serum-free medium with R8-LP. After a 1-h incubation under 5% CO_2/air at 37 °C, the cells were washed with ice-cold PBS (−), and further incubated in medium with 10% serum for 1 h in the absence of R8-LP. After incubation, MitoFluor Red 589 (Molecular Probes; Eugene, OR, USA) was applied to the medium at a final concentration of 100 nM to stain the mitochondria. After incubation for 20 min, the cells were washed with ice-cold PBS (−) and then observed by confocal laser scanning microscopy (LSM510 or LSM510 META; Carl Zeiss Co. Ltd., Jena, Germany).

2.10. Intracellular observation using confocal laser scanning microscopy

R8-LPs encapsulating GFP or labeled with 1 mol% NBD–DOPE were incubated with HeLa cells (final lipid concentration, 13.5 μM) to observe the intracellular trafficking of encapsulated GFP (Fig. 4A) or the carriers themselves (Fig. 4B). The cells were excited by 488 nm and 568 nm light from an Ar/Kr laser. A series of images were obtained using an LSM510 with a water immersion objective lens (Achroplan 63x/NA=0.95) and a dichroic mirror (HFT488/568). The two fluorescence detection channels (Ch) were set to the following filters: Ch1: LP585 (red); Ch 2: BP 505–550 (green).

2.11. Intracellular observation of Gold Colloid encapsulated in MITO-Porter using transmission electron microscopy

HeLa cells (1×10^5 cells/mL) were cultured in 100-mm tissue culture dishes with D'MEM, which contained 10% FBS, under 5% CO_2/air at 37 °C for 24 h. The cells were washed with ice-cold PBS (−) and incubated in 5 mL of serum-free medium, which contained R8-LP encapsulating Gold Colloid to a final lipid concentration of 50 μM. After a 1-h incubation under 5% CO_2/air at 37 °C, the cells were washed 3 times with ice-cold PBS (−), and further incubated in medium with 10% serum for 1 h in the absence of R8-LP.

Transmission electron microscopy analysis of cells treated with various liposomes was carried out essentially as described previously [27,28]. Cells treated with liposomes were detached with 0.05% trypsin–0.03% EDTA and then pelleted by centrifugation at 200 ×*g* for 3 min. After centrifugation, the cells were fixed in cacodylate buffer (0.05 M cacodylate, pH 7.4) supplemented with 250 mM sucrose and 1% glutaraldehyde. After a 1-h incubation at 4 °C, the fixed cells were again centrifuged at 200 ×*g* for 5 min and then postfixed in cacodylate buffer supplemented with 0.5% OsO_4. After a 1-h incubation at 4 °C, the cells were dehydrated in a graded series of ethanol and embedded in TAAB EPON 812 RESIN (TAAB Laboratories Equipment Ltd; Berkshire, England). Ultrathin sections were stained with uranyl acetate and lead citrate and examined by transmission electron microscopy with a Hitachi H-800MT electron microscope (Hitachi High-Tech Science Systems Corporation; Ibaraki, Japan).

2.12. Evaluation of membrane fusion in living cells using spectral imaging fluorescent microscopy

R8-LPs were prepared with 1 mol% NBD–DOPE (excitation at 460 nm and emission at 534 nm) and 0.5 mol% rhodamine–DOPE (excitation at 550 nm and emission at 590 nm) as a donor and an acceptor of FRET, respectively. The dual-labeled liposomes were incubated with HeLa cells (final lipid concentration, 5.4 μM). Mitochondria were additionally stained with MitoFluor Red 589 (excitation at 588 nm and emission at 622 nm). The cells were observed using an LSM510 META equipped with an oil-immersion objective lens (Plan-Apochromat 63x/NA=1.4). To evaluate membrane fusion between the carriers and mitochondria, NBD was excited by light (488 nm) derived from an argon laser. Emitted light filtered through a dichroic mirror (HFT488) was spectroscopically analyzed (510–630 nm) as shown in Fig. 6 (A,D). Through the spectra ranges used in the analysis, background fluorescence derived from the emission from rhodamine and MitoFluor Red 589 was negligible when they were excited at 488 nm (data not shown). Fluorescence spectra of R.O.I. (region of image) were selected Fig. 6 (A,D) and the emission at each wavelength were normalized to the rhodamine peak fluorescence intensity (emission at 590 nm) as shown in Fig. 6 (C,F).

To identify the localization of liposomes on the mitochondria, images were further obtained by spectral images ranging from 570 to 630 nm with a He/Ne laser (543 nm) using a dichroic mirror (HFT UV/488/543/633) as shown in Fig. 6 (B,E). Liposomes (yellow) and mitochondria (red) can be clearly distinguished since the emission spectral peak of MitoFluor Red 589 was detected at the far-red region (emission at 622 nm) compared with that of rhodamine (emission at 590 nm).

To further evaluate membrane fusion of the carriers, the relative intensity of fluorescence on and outside the mitochondria was estimated (Fig. 7). Relative intensity represents reduction of energy transfer as a function of membrane fusion. Based on images, when the carriers were excited by light of 488 nm, the relative intensity was calculated by as follows:

$$\text{relative intensity} = F_{530}/F_{590} \quad (3)$$

where F_{530} and F_{590} represent the fluorescence intensity of carriers at 530 nm and 590 nm, respectively.

3. Results

3.1. Screening for fusogenic liposomes to the mitochondrial membrane

To deliver cargos into mitochondria in our strategy, the liposomes must fuse with the mitochondrial membrane. Although the R8-LPs composed of DOPE and CHEMS can deliver pDNA to the nucleus efficiently [29], these lipids may not be the best lipid composition for mitochondria. Therefore, we screened liposomes with different lipid compositions for their ability to fuse with the mitochondrial membrane. Table 1 summarizes the sizes of the liposomes. The diameters were comparable (approximately 200–300 nm). Overall, the zeta potentials of the neutral lipid-containing liposomes, the anionic lipid-containing liposomes, and the R8-LPs were approximately 0 mV, −50 mV, and +50 mV, respectively.

These liposomes were incubated with isolated rat liver mitochondria and their fusogenic activity was measured using FRET. As shown in Fig. 2, R8-LPs composed of DOPE (R8-DOPE-LPs), which is a fusogenic lipid commonly used in drug delivery, showed higher fusogenic activities than R8-LPs composed of egg yolk phosphatidyl choline (R8-EPC-LPs). In the absence of R8 surface modification, binding of the liposomes to mitochondria is considerably reduced, suggesting that a strong electrostatic binding between R8-LPs and mitochondria stimulates the fusogenic activity of liposomes, and especially those containing DOPE. R8-DOPE-LPs also containing SM or PA exhibited the highest fusion activities among the lipids examined. Based on these results, we named the R8-DOPE-LPs containing either SM or PA as MITO-Porters.

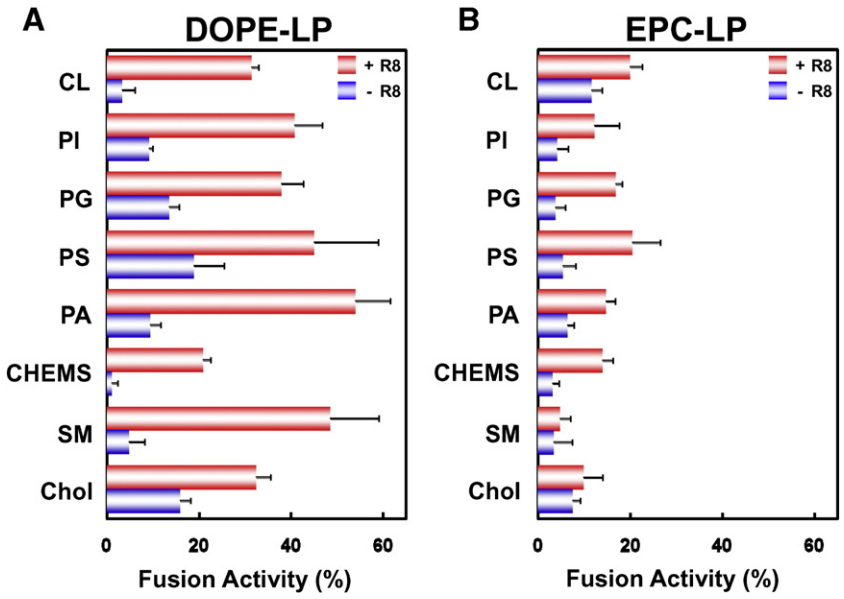

Fig. 2. Screening of fusogenic lipid composition with the mitochondrial membrane. Labeled liposomes were incubated with isolated rat liver mitochondria for 30 min at 25 °C. After incubation, energy transfer was assessed by the fluorescence intensity. Fusion activities (%) of DOPE-LP (A) and EPC-LP (B) were calculated in terms of reduction of FRET as described in the Materials and methods section. Data are presented as a mean of triplicates. Red bars, R8-LP; blue bars, unmodified liposome. DOPE, 1,2-dioleoyl-*sn*-glycero-3-phosphatidyl ethanolamine; EPC, egg yolk phosphatidyl choline; CL, cardiolipin; PI, phosphatidyl inositol; PG, phosphatidyl glycerol; PS, phosphatidyl serine; PA, phosphatidic acid; CHEMS, cholesteryl hemisuccinate (5-cholesten-3-ol 3-hemisuccinate); SM, sphingomyelin; Chol, cholesterol. Data are represented by the mean ± S.D. (n = 3).

3.2. Evaluation of macromolecule delivery in isolated rat liver mitochondria

We next examined whether the MITO-Porters could deliver macromolecules to the mitochondria by passing through the OM of mitochondria. GFP was encapsulated into the MITO-Porter and incubated with isolated rat liver mitochondria. After the mitochondria were fractionated into OM and IMS fractions, GFP was detected by Western blotting. As shown in Fig. 3A, in the case of MITO-Porter, GFP was detected in both the OM and IMS fractions (lanes 3–6), while in the case of R8-EPC-LP (low fusion activity), GFP was detected only in the OM fraction (lanes 7–10). These results indicated that MITO-Porter could deliver macromolecules into mitochondria, while R8-EPC-LP could only bind to the OM and failed to deliver GFP into mitochondria. GFP was not detected in either the OM or IMS fractions when GFP alone was incubated with isolated rat liver mitochondria (Fig. 3A, lanes 1,2). This result suggested that the packaging of GFP in MITO-Porter is an important process, although the encapsulation efficiency of MITO-Porter was not high (approximately 1%).

Unexpectedly, the molecular weight of GFP detected in the IMS fraction (28 kDa) was smaller than that of the full-length molecule (33 kDa), which suggested the possibility that GFP was cleaved by a protease(s) in the IMS. To test this, we incubated purified GFP with either the IMS fraction or IB, and then subjected the reactions to Western blotting. As predicted, the molecular weight of GFP incubated in the IMS fraction was 28 kDa, whereas it remained intact when incubated in IB (Fig. 3B). Furthermore, it is noteworthy that the cleavage site must be far from the active center of GFP (25 kDa) [30],

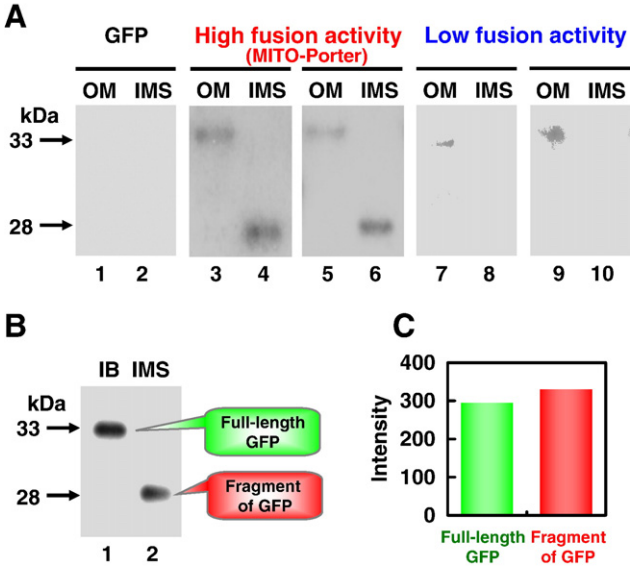

Fig. 3. Mitochondrial delivery of GFP with MITO-Porter. A, GFP was detected in isolated rat liver mitochondria using Western blotting as follows: lanes 1,2, GFP alone; lanes 3,4, MITO-Porter (SM) [R8-DOPE/SM-LP]; lanes 5,6, MITO-Porter (PA) [R8-DOPE/PA-LP]; lanes 7,8, R8-EPC/SM-LP; lanes 9,10, R8-EPC/PA-LP. Bands observed at 33 kDa and 28 kDa represent the full-length GFP (lanes 3,5,7,9) and the fragment of GFP (lanes 4,6), respectively. OM (lanes 1,3,5,7,9) and IMS (lanes 2,4,6,8,10) indicate outer membrane fraction and intermembrane space fraction, respectively. B, GFP was added either to the IMS (lane 1) or to isolation buffer (IB) (lane 2) and then incubated at 25 °C for 30 min (final GFP concentration, 1 ng/μL). After incubation, a 2.5 μL aliquot of each sample was subjected to Western blotting. C, Comparison of the fluorescence intensity between full-length GFP and the fragment of GFP.

because the truncated protein retained its ability to fluoresce (Fig. 3C). These results support the assertion that the MITO-Porter delivered its GFP cargo to the IMS by passing through the OM.

3.3. Intracellular observation of MITO-Porters by confocal laser scanning microscopy

The ability of MITO-Porter to deliver macromolecules into mitochondria was examined in living HeLa cells using confocal laser scanning microscopy. GFP, which is an aqueous phase marker, was encapsulated in MITO-Porter. When living cells were treated with GFP alone, we could not observe GFP in those cells (data not shown). In the case of MITO-Porter, GFP (green) was seen to co-localize with mitochondria (stained red with MitoFluor Red 589), observed as a yellow signal in the merged images (Fig. 4A (a),(b)). Yellow clusters were seen in several different cells (see Supplementary data, Fig. S1). Approximately 10% of the cells possessed GFP-positive mitochondria. On the other hand, little co-localization was observed in the case of the R8-EPC-LP control carrier (Fig. 4A (c)). No co-localization between GFP and mitochondria in images from at least 30 different cells was observed (data not shown). We expected to see a diffused GFP signal in mitochondria in the case of the MITO-Porter; however, we actually observed yellow clusters (Fig. 4A (a),(b)). These results could be explained by the fact that mitochondria are compartmentalized in living cells [31] and GFP delivered by MITO-Porter may not be able to diffuse into other compartments.

Similar results were also found for the intracellular distribution of the carriers themselves (Fig. 4B). In the case of the MITO-Porter, several yellow clusters were observed (Fig. 4B (a),(b)), indicating that the MITO-Porters (green) are co-localized with mitochondria (red). These results suggested that the lipid of the MITO-Porter had accumulated in mitochondria. In contrast, in the case of R8-EPC-LP, only green clusters were observed (Fig. 4B (c)). It is likely that R8-EPC-LPs failed to fuse with the mitochondrial membrane, even though they could be delivered close to the mitochondria. Furthermore, when MITO-Porter was added to homogenate from HeLa cells, approximately 20% of the MITO-Porter bound to mitochondria while most remained in the cytosol fraction (data not shown). This result was consistent with that of the confocal laser scanning microscopy analyses, as shown in the Fig. 4, where some but not all of the MITO-Porters accumulated at mitochondria within cells.

3.4. Observation of macromolecule delivery to mitochondria in living cells using transmission electron microscopy

Transmission electron microscopy analysis was also performed to provide evidence that MITO-Porter can deliver macromolecules into mitochondria of living cells. Colloidal gold particles with a diameter of approximately 10 nm were

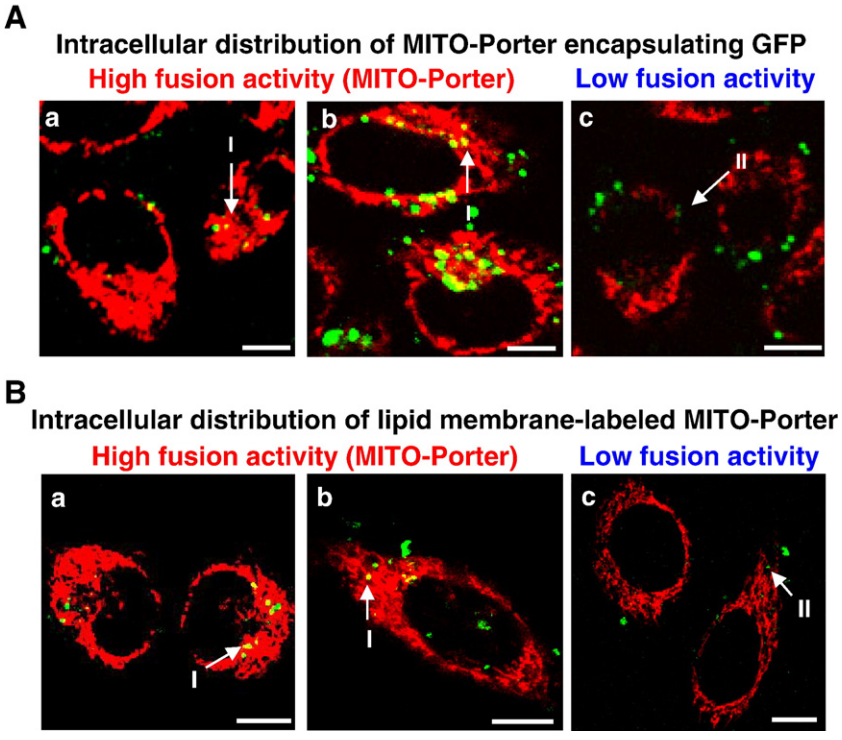

Fig. 4. Intracellular observation of MITO-Porter using confocal laser scanning microscopy. MITO-Porter (SM) [R8-DOPE/SM-LP] (a), MITO-Porter (PA) [R8-DOPE/PA-LP] (b), and R8-EPC/Chol-LP (c) encapsulating GFP as an aqueous phase marker (A), or labeled with NBD–DOPE as a tracer of the carrier (B) were incubated with HeLa cells at 37 °C for 1 h. After the medium had been replaced, the cells were further incubated for 1 h in the absence of the carriers. Mitochondria were stained with MitoFluor Red 589 prior to observation by confocal laser scanning microscopy. The clusters present in the mitochondria and cytosol are indicated as I or II, respectively. Scale bar, 10 μm.

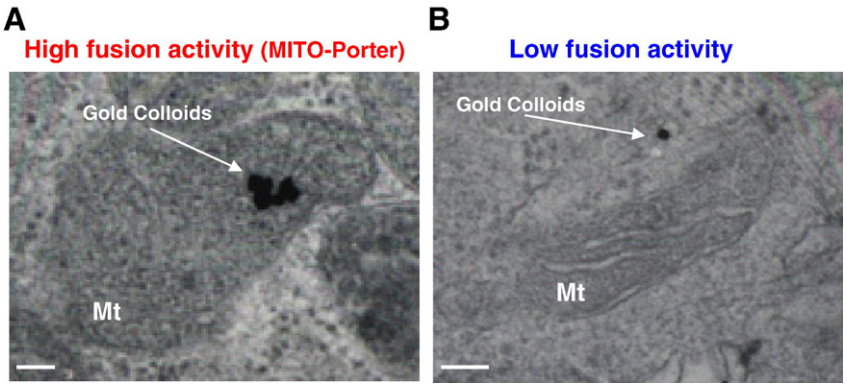

Fig. 5. Transmission electron microscopy observation of mitochondrial delivery in living cells. MITO-Porter (SM) [R8-DOPE/SM-LP] (A) and R8-EPC/SM-LP (B) encapsulating Gold Colloid (8–12 nm in diameter) as a model macromolecule were incubated with HeLa cells at 37 °C for 1 h. After the medium had been replaced, the cells were further incubated for 1 h in the absence of the carriers, and then the cells were observed by transmission electron microscopy as described in the Materials and methods section. Mt indicates mitochondria. Scale bars, 100 nm.

used as model macromolecules and were encapsulated in MITO-Porter, and R8-EPC-LP was used as a control. MITO-Porter successfully delivered colloidal gold particles into mitochondria while R8-EPC-LP did not (Fig. 5). These results provide further support that MITO-Porter is able to deliver large molecular weight cargoes into the intra-mitochondrial compartment in living cells.

3.5. Evaluation of membrane fusion with mitochondria in living cells using spectral imaging fluorescent microscopy

To obtain more direct evidence that MITO-Porter can deliver macromolecules into mitochondria via membrane fusion, we performed FRET analysis in living cells using a spectral imaging fluorescence microscopy system [32]. FRET analysis is

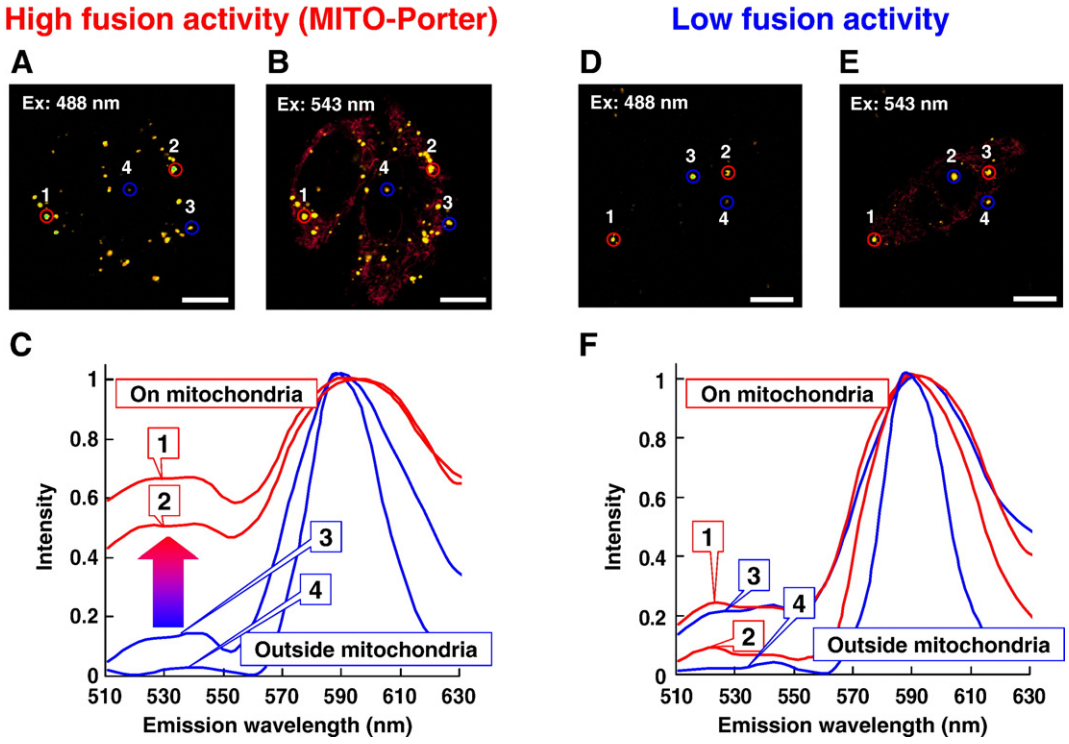

Fig. 6. Membrane fusion evaluation between MITO-Porter and mitochondria in living cells by FRET analysis using spectral imaging fluorescence microscopy. MITO-Porter (SM) [R8-DOPE/SM-LP] (A–C) and R8-EPC/SM-LP (D–F) were prepared with both NBD–DOPE and rhodamine–DOPE. Next, they were incubated with HeLa cells followed by observation using confocal laser scanning microscopy as described in the Materials and methods section. (A,D) Spectral image figures were observed in the case of excitation at 488 nm to evaluate membrane fusion by FRET. (B,E) Spectral image figures were observed in the case of excitation at 543 nm to identify the localization of liposomes (yellow color) and mitochondria (red color). (C,F) Fluorescence spectra of R.O.I. (region of image) were selected from A and D and the emission were normalized to the rhodamine peak fluorescence intensity. The spectra present on and outside the mitochondria are indicated as red or blue lines, respectively. In the non-fusogenic state, emission energy of NBD (donor) is transferred to the excitation energy of rhodamine (acceptor). As a result, the fluorescence intensity of NBD at 530 nm was minimized. Lipid mixing by membrane fusion between the labeled liposome and mitochondrial membrane will lead to the diffusion of the donor and acceptor; this results in a reduction of FRET and an increase in the fluorescence intensity at 530 nm. Scale bars, 10 μm.

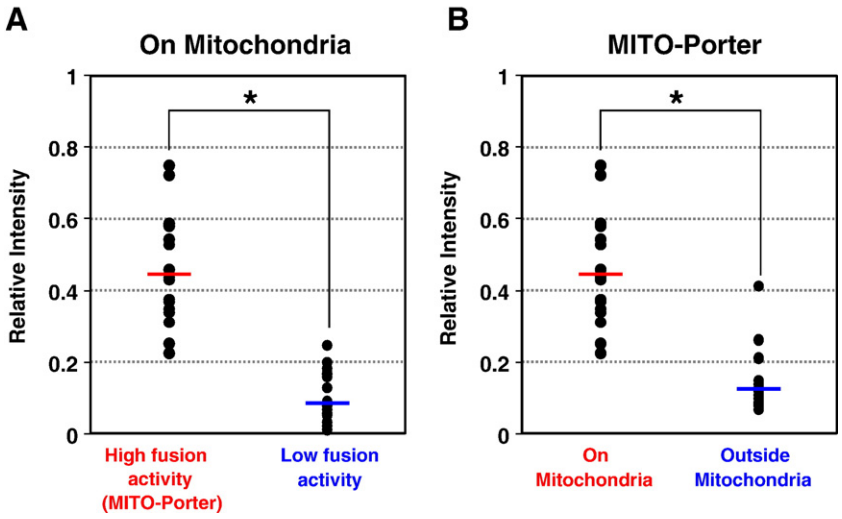

Fig. 7. Statistical analysis of the membrane fusion activity of MITO-Porter on and outside mitochondria. Based on images observed by spectral imaging fluorescence microscopy, as shown in Fig.6, the relative intensity, which represents the fraction of membrane fusion, was calculated as described in Materials and methods. Bars represent the mean values ($n=20$). Asterisks indicate significant differences determined by the Student's t-test ($p<0.001$). A, Relative intensity of MITO-Porter (SM) [R8-DOPE/SM-LP] and R8-EPC/SM-LP on mitochondria are shown. B, Relative intensity of MITO-Porter (SM) [R8-DOPE/SM-LP] on and outside mitochondria are shown.

often used to detect protein interactions in living cells [33]. In this study, we applied this method to evaluate membrane fusion. Liposomal membranes were labeled with both NBD–DOPE (excitation at 460 nm and emission at 534 nm) and rhodamine–DOPE (excitation at 550 nm and emission at 590 nm) so that energy transfer will occur from NBD to rhodamine. As shown in Fig. 6, the fluorescence intensity at 530 nm increased significantly, which indicated reduction of energy transfer due to fusion between the liposomal and mitochondrial membranes in the case of MITO-Porter. On the other hand, no such increase at 530 nm was detected in the case of R8-EPC-LP both on the surface and outside the mitochondria.

We next estimated the relative intensity as described in Materials and methods to statistically evaluate membrane fusion of MITO-Porter and R8-EPC-LP on and outside the mitochondria (Fig. 7). On mitochondria, MITO-Porter showed higher fusogenic activities than R8-EPC-LP (Fig. 7A). Moreover, MITO-Porter could efficiently induce membrane fusion on the mitochondria compared with outside the mitochondria (Fig. 7B). These results are consistent with our concept that MITO-Porter can deliver macromolecules into mitochondria via membrane fusion in living cells.

4. Discussion

A variety of peptides called protein transduction domains (PTDs), such as human immunodeficiency virus (HIV-1) TAT-(48-60) and Antennapedia-(43–58), have been reported to efficiently deliver biologically active agents to a variety of cells [34–36]. PTDs have been employed to deliver oligonucleotides, peptides, and full-length proteins [37]. Moreover, V.P. Torchilin et al. recently demonstrated that certain TAT-linked liposomes, even with a diameter of 200 nm, could be efficiently internalized into a variety of cell lines in intact form [38]. Recently published reports suggest that the arginine residues of the TAT peptide play a critical role in enhancing the cellular uptake of TAT, and arginine homopolymers exhibited higher transduction efficiency than the TAT peptide [39–41]. These findings have led to increased focus on arginine homopolymers and synthetic peptide analogues of arginine as transduction domains such as R7 [39], R8 [41,42], R9 [40,43], and R11 [44–46].

S. Futaki et al. reported that R8 delivered exogenous protein into cells as efficiently as TAT peptide based on the fluorescence microscopic observation of the fluorescein-labeled peptides [41]. Moreover, they showed that these peptides internalized into cells within 5 min, with little inhibition of uptake at 4 °C, suggesting that these peptides share a similar in internalization mechanism, which is macropinocytosis, a clathrin-independent endocytosis [41,42]. We also showed that high-density R8-LPs are taken up mainly through macropinocytosis, and delivered to the cytosol retaining the aqueous phase marker [18]. Based on these previous reports, R8 was chosen as a cytosol delivery device for MITO-Porter.

As shown in Fig. 4, R8-EPC-LP could not deliver cargos to mitochondria in living cells. In this paper, we insisted on mitochondrial membrane fusion as an important factor for mitochondrial delivery. However, failure of mitochondrial delivery by R8-EPC-LP might result from something other than a lack of mitochondrial membrane fusion. To achieve mitochondrial delivery in living cells, the carrier must be internalized into cell (i). Thereafter, intracellular trafficking of the carrier including endosomal escape (ii) and subsequent mitochondrial delivery (iii), must be accomplished. If these processes were inhibited by EPC lipid, then R8-EPC-LP could not achieve mitochondrial delivery. Here, we discuss these points as follows.

First, we were concerned about the possibility that EPC might prevent cellular uptake of R8. We previously reported that macropinocytosis is the major entrance pathway for high-density R8-LPs and that the lipid composition had no effect on the internalization mechanism [18]. Therefore, we have recognized

that efficiencies of cellular uptake of MITO-Porter and R8-EPC-LP are similar. Second, in general, liposomes including DOPE can escape from the endosome more efficiently than those including EPC [47]. However, modification with a high density of R8 causes liposomes to internalize into cells mainly through macropinocytosis and enhances endosomal escape even in the case of low fusogenic liposomes [18]. Third, EPC significantly reduced mitochondrial membrane fusion activity in the case of isolated mitochondria, as shown in Fig. 2. This result suggested that EPC could inhibit membrane fusion with mitochondria in living cells. Therefore, we concluded that EPC drastically inhibited membrane fusion with mitochondria and partially lowered endosomal escape, and that these factors are likely to be involved in the low level of mitochondrial delivery in living cells.

MITO-Porter contained R8, which has a positive charge. Therefore, MITO-Porter might be rapidly eliminated from the systemic circulation after intravenous administration, owing to the high rate of clearance by the reticuloendothelial system (RES) or other organs, as also found with cationic liposomes [48,49]. It is generally accepted that extended circulation can be achieved by the surface modification of carriers with poly (ethylene glycol) (PEG) [49,50]. However, PEG is undesirable during cellular uptake and subsequent processes [51]. We have recently reported the development of a PEG–Peptide–DOPE conjugate (PPD) for cancer gene therapy in vivo [52]. In this strategy, the PEG is removed from the carriers via cleavage by a matrix metalloproteinase, which is specifically expressed in tumor tissues. In vivo studies revealed that the PPD was potent in stabilizing the carriers in the systemic circulation and facilitating tumor accumulation. Moreover, the intravenous administration of PPD-modified gene carrier resulted in the stimulation of gene expression in tumor tissue. In the future, we will attempt to develop a mitochondrial delivery system for intravenous administration using PPD-modified MITO-Porter.

In this study, we described a liposome-based carrier system named MITO-Porter which can deliver macromolecules into mitochondria via a membrane fusion mechanism. Entry of the intact carriers into cells is stimulated by R8 on the surface of the MITO-Porter, and delivery into mitochondria is facilitated by the MITO-Porter's fusogenic lipid composition. Delivery of macromolecular cargoes to mitochondria was evaluated by confocal laser scanning microscopy and transmission electron microscopy. FRET analysis using spectral imaging fluorescence microscopy indicated that MITO-Porter delivery occurs via a membrane fusion mechanism in living cells. These results demonstrated the principle of our mitochondrial delivery system, which could lead to development of a novel drug carrier. In the future, we will attempt to improve MITO-Porter in terms of mitochondrial targeting efficiency and in vivo delivery for mitochondrial diseases therapy. Studies directed at these goals are currently in progress.

Acknowledgements

The authors thank Prof. S. Futaki (Kyoto University) for providing STR-R8 and also Dr. Daryl Henderson for his helpful advice in writing the English manuscript. This work was supported in part by Grants-in-Aid for Exploratory Research from the Ministry of Education, Culture, Sports, Science and Technology of Japan.

Appendix A. Supplementary data

Supplementary data associated with this article can be found, in the online version, at doi:10.1016/j.bbamem.2007.11.002.

References

[1] A.H. Schapira, Mitochondrial disease, Lancet 368 (2006) 70–82.
[2] D.C. Chan, Mitochondria: dynamic organelles in disease, aging, and development, Cell 125 (2006) 1241–1252.
[3] Y. Yamada, H. Akita, K. Kogure, H. Kamiya, H. Harashima, Mitochondrial drug delivery and mitochondrial disease therapy—an approach to liposome-based delivery targeted to mitochondria, Mitochondrion 7 (2007) 63–71.
[4] V. Weissig, S.M. Cheng, G.G. D'Souza, Mitochondrial pharmaceutics, Mitochondrion 3 (2004) 229–244.
[5] V. Weissig, V.P. Torchilin, Cationic bolasomes with delocalized charge centers as mitochondria-specific DNA delivery systems, Adv. Drug Deliv. Rev. 49 (2001) 127–149.
[6] G.G. D'Souza, R. Rammohan, S.M. Cheng, V.P. Torchilin, V. Weissig, DQAsome-mediated delivery of plasmid DNA toward mitochondria in living cells, J. Control. Release 92 (2003) 189–197.
[7] I.A. Khalil, K. Kogure, H. Akita, H. Harashima, Uptake pathways and subsequent intracellular trafficking in nonviral gene delivery, Pharmacol. Rev. 58 (2006) 32–45.
[8] Y. Yoneda, T. Semba, Y. Kaneda, R.L. Noble, Y. Matsuoka, T. Kurihara, Y. Okada, N. Imamoto, A long synthetic peptide containing a nuclear localization signal and its flanking sequences of SV40 T-antigen directs the transport of IgM into the nucleus efficiently, Exp. Cell Res. 201 (1992) 313–320.
[9] M. Tanimoto, H. Kamiya, N. Minakawa, A. Matsuda, H. Harashima, No enhancement of nuclear entry by direct conjugation of a nuclear localization signal peptide to linearized DNA, Bioconjug. Chem. 14 (2003) 1197–1202.
[10] T. Nagasaki, T. Myohoji, T. Tachibana, S. Futaki, S. Tamagaki, Can nuclear localization signals enhance nuclear localization of plasmid DNA? Bioconjug. Chem. 14 (2003) 282–286.
[11] G. Schatz, 17th Sir Hans Krebs lecture. Signals guiding proteins to their correct locations in mitochondria, Eur. J. Biochem. 165 (1987) 1–6.
[12] S.M. Gasser, G. Daum, G. Schatz, Import of proteins into mitochondria. Energy-dependent uptake of precursors by isolated mitochondria, J. Biol. Chem. 257 (1982) 13034–13041.
[13] D. Vestweber, G. Schatz, DNA-protein conjugates can enter mitochondria via the protein import pathway, Nature 338 (1989) 170–172.
[14] M. Seibel, C. Bachmann, J. Schmiedel, N. Wilken, F. Wilde, H. Reichmann, G. Isaya, P. Seibel, D. Pfeiler, Processing of artificial peptide-DNA-conjugates by the mitochondrial intermediate peptidase (MIP), Biol. Chem. 380 (1999) 961–967.
[15] A. Flierl, C. Jackson, B. Cottrell, D. Murdock, P. Seibel, D.C. Wallace, Targeted delivery of DNA to the mitochondrial compartment via import sequence-conjugated peptide nucleic acid, Mol. Ther. 7 (2003) 550–557.
[16] N. Wiedemann, A.E. Frazier, N. Pfanner, The protein import machinery of mitochondria, J. Biol. Chem. 279 (2004) 14473–14476.
[17] T. Endo, Y. Nakayama, M. Nakai, Avidin fusion protein as a tool to generate a stable translocation intermediate spanning the mitochondrial membranes, J. Biochem. (Tokyo) 118 (1995) 753–759.
[18] I.A. Khalil, K. Kogure, S. Futaki, H. Harashima, High density of octaarginine stimulates macropinocytosis leading to efficient intracellular trafficking for gene expression, J. Biol. Chem. 281 (2006) 3544–3551.
[19] R. Suzuki, Y. Yamada, H. Harashima, Efficient cytoplasmic protein delivery by means of a multifunctional envelope-type nano device, Biol. Pharm. Bull. 30 (2007) 758–762.
[20] R. Galovic Rengel, K. Barisic, Z. Pavelic, T. Zanic Grubisic, I. Cepelak, J. Filipovic-Grcic, High efficiency entrapment of superoxide dismutase into mucoadhesive chitosan-coated liposomes, Eur. J. Pharm. Sci. 15 (2002) 441–448.

[21] Y. Shinohara, M.R. Almofti, T. Yamamoto, T. Ishida, F. Kita, H. Kanzaki, M. Ohnishi, K. Yamashita, S. Shimizu, H. Terada, Permeability transition-independent release of mitochondrial cytochrome *c* induced by valinomycin, Eur. J. Biochem. 269 (2002) 5224–5230.
[22] Y. Shinohara, I. Sagawa, J. Ichihara, K. Yamamoto, K. Terao, H. Terada, Source of ATP for hexokinase-catalyzed glucose phosphorylation in tumor cells: dependence on the rate of oxidative phosphorylation relative to that of extramitochondrial ATP generation, Biochim. Biophys. Acta 1319 (1997) 319–330.
[23] T. Kakudo, S. Chaki, S. Futaki, I. Nakase, K. Akaji, T. Kawakami, K. Maruyama, H. Kamiya, H. Harashima, Transferrin-modified liposomes equipped with a pH-sensitive fusogenic peptide: an artificial viral-like delivery system, Biochemistry 43 (2004) 5618–5628.
[24] D.K. Struck, D. Hoekstra, R.E. Pagano, Use of resonance energy transfer to monitor membrane fusion, Biochemistry 20 (1981) 4093–4099.
[25] O. Maier, V. Oberle, D. Hoekstra, Fluorescent lipid probes: some properties and applications (a review), Chem. Phys. Lipids 116 (2002) 3–18.
[26] J.W. Greenawalt, The isolation of outer and inner mitochondrial membranes, Methods Enzymol. 31 (1974) 310–323.
[27] S. Terauchi, T. Yamamoto, K. Yamashita, M. Kataoka, H. Terada, Y. Shinohara, Molecular basis of morphological changes in mitochondrial membrane accompanying induction of permeability transition, as revealed by immuno-electron microscopy, Mitochondrion 5 (2005) 248–254.
[28] A. Anshup, J.S. Venkataraman, C. Subramaniam, R.R. Kumar, S. Priya, T.R. Kumar, R.V. Omkumar, A. John, T. Pradeep, Growth of gold nanoparticles in human cells, Langmuir 21 (2005) 11562–11567.
[29] I.A. Khalil, K. Kogure, S. Futaki, S. Hama, H. Akita, M. Ueno, H. Kishida, M. Kudoh, Y. Mishina, K. Kataoka, M. Yamada, H. Harashima, Octaarginine-modified multifunctional envelope-type nanoparticles for gene delivery, Gene Ther. 14 (2007) 682–689.
[30] X. Li, G. Zhang, N. Ngo, X. Zhao, S.R. Kain, C.C. Huang, Deletions of the *Aequorea victoria* green fluorescent protein define the minimal domain required for fluorescence, J. Biol. Chem. 272 (1997) 28545–28549.
[31] V.P. Skulachev, Mitochondrial filaments and clusters as intracellular power-transmitting cables, Trends Biochem. Sci. 26 (2001) 23–29.
[32] T. Haraguchi, T. Shimi, T. Koujin, N. Hashiguchi, Y. Hiraoka, Spectral imaging fluorescence microscopy, Genes Cells 7 (2002) 881–887.
[33] A. Miyawaki, J. Llopis, R. Heim, J.M. McCaffery, J.A. Adams, M. Ikura, R.Y. Tsien, Fluorescent indicators for Ca^{2+} based on green fluorescent proteins and calmodulin, Nature 388 (1997) 882–887.
[34] A. Joliot, A. Prochiantz, Transduction peptides: from technology to physiology, Nat. Cell Biol. 6 (2004) 189–196.
[35] H. Nagahara, A.M. Vocero-Akbani, E.L. Snyder, A. Ho, D.G. Latham, N.A. Lissy, M. Becker-Hapak, S.A. Ezhevsky, S.F. Dowdy, Transduction of full-length TAT fusion proteins into mammalian cells: TAT-p27Kip1 induces cell migration, Nat. Med. 4 (1998) 1449–1452.
[36] S.R. Schwarze, A. Ho, A. Vocero-Akbani, S.F. Dowdy, In vivo protein transduction: delivery of a biologically active protein into the mouse, Science 285 (1999) 1569–1572.
[37] J.S. Wadia, S.F. Dowdy, Protein transduction technology, Curr. Opin. Biotechnol. 13 (2002) 52–56.
[38] V.P. Torchilin, R. Rammohan, V. Weissig, T.S. Levchenko, TAT peptide on the surface of liposomes affords their efficient intracellular delivery even at low temperature and in the presence of metabolic inhibitors, Proc. Natl. Acad. Sci. U. S. A. 98 (2001) 8786–8791.
[39] J.B. Rothbard, S. Garlington, Q. Lin, T. Kirschberg, E. Kreider, P.L. McGrane, P.A. Wender, P.A. Khavari, Conjugation of arginine oligomers to cyclosporin A facilitates topical delivery and inhibition of inflammation, Nat. Med. 6 (2000) 1253–1257.
[40] P.A. Wender, D.J. Mitchell, K. Pattabiraman, E.T. Pelkey, L. Steinman, J.B. Rothbard, The design, synthesis, and evaluation of molecules that enable or enhance cellular uptake: peptoid molecular transporters, Proc. Natl. Acad. Sci. U. S. A. 97 (2000) 13003–13008.
[41] S. Futaki, T. Suzuki, W. Ohashi, T. Yagami, S. Tanaka, K. Ueda, Y. Sugiura, Arginine-rich peptides. An abundant source of membrane-permeable peptides having potential as carriers for intracellular protein delivery, J. Biol. Chem. 276 (2001) 5836–5840.
[42] T. Suzuki, S. Futaki, M. Niwa, S. Tanaka, K. Ueda, Y. Sugiura, Possible existence of common internalization mechanisms among arginine-rich peptides, J. Biol. Chem. 277 (2002) 2437–2443.
[43] H. Mitsui, T. Inozume, R. Kitamura, N. Shibagaki, S. Shimada, Polyarginine-mediated protein delivery to dendritic cells presents antigen more efficiently onto MHC class I and class II and elicits superior antitumor immunity, J. Invest. Dermatol. 126 (2006) 1804–1812.
[44] M. Matsushita, K. Tomizawa, A. Moriwaki, S.T. Li, H. Terada, H. Matsui, A high-efficiency protein transduction system demonstrating the role of PKA in long-lasting long-term potentiation, J. Neurosci. 21 (2001) 6000–6007.
[45] H. Noguchi, M. Matsushita, T. Okitsu, A. Moriwaki, K. Tomizawa, S. Kang, S.T. Li, N. Kobayashi, S. Matsumoto, K. Tanaka, N. Tanaka, H. Matsui, A new cell-permeable peptide allows successful allogeneic islet transplantation in mice, Nat. Med. 10 (2004) 305–309.
[46] H. Noguchi, Y. Nakai, S. Matsumoto, M. Kawaguchi, M. Ueda, T. Okitsu, Y. Iwanaga, Y. Yonekawa, H. Nagata, K. Minami, Y. Masui, S. Futaki, K. Tanaka, Cell permeable peptide of JNK inhibitor prevents islet apoptosis immediately after isolation and improves islet graft function, Am. J. Transplant 5 (2005) 1848–1855.
[47] H. Farhood, N. Serbina, L. Huang, The role of dioleoyl phosphatidylethanolamine in cationic liposome mediated gene transfer, Biochim. Biophys. Acta 1235 (1995) 289–295.
[48] B.M. Tandia, M. Vandenbranden, R. Wattiez, Z. Lakhdar, J.M. Ruysschaert, A. Elouahabi, Identification of human plasma proteins that bind to cationic lipid/DNA complex and analysis of their effects on transfection efficiency: implications for intravenous gene transfer, Mol. Ther. 8 (2003) 264–273.
[49] V.P. Torchilin, Recent advances with liposomes as pharmaceutical carriers, Nat. Rev. Drug Discov. 4 (2005) 145–160.
[50] T.M. Allen, C. Hansen, Pharmacokinetics of stealth versus conventional liposomes: effect of dose, Biochim. Biophys. Acta 1068 (1991) 133–141.
[51] S. Mishra, P. Webster, M.E. Davis, PEGylation significantly affects cellular uptake and intracellular trafficking of non-viral gene delivery particles, Eur. J. Cell Biol. 83 (2004) 97–111.
[52] H. Hatakeyama, H. Akita, K. Kogure, M. Oishi, Y. Nagasaki, Y. Kihira, M. Ueno, H. Kobayashi, H. Kikuchi, H. Harashima, Development of a novel systemic gene delivery system for cancer therapy with a tumor-specific cleavable PEG-lipid, Gene Ther. 14 (2007) 68–77.